Proc. Estonian Acad. Sci. Phys. Math., 1992, 41, 1, 49—62
https://doi.org/10.3176/phys.math.1992.1.07

UDC 535.377; 537.635

Toomas RÕÕM and Georg LIIDJA**

PARAMAGNETIC RESONANCE OF ELECTRONS TRAPPED ON HYDROGEN AND THERMOLUMINESCENCE OF CaO CRYSTALS

During irradiation of additively colored CaO crystals into the F absorption band at liquid helium temperature paramagnetic $S=1/2$, $I=1/2$ centers arise having tetragonal symmetry and spin Hamiltonian parameters $g_{\parallel}=1.9996\pm0.0001$, $g_{\perp}=2.0005\pm0.0001$, $A_{\parallel}=40.3\pm1.6$ MHz, $A_{\perp}=20.9\pm0.8$ MHz, and nuclear g-factor of the proton $g_N=5.6\pm0.2$. The paramagnetic centers are formed by electron trapping at impurity hydrogen ions H^- which replace oxygen ions O^{2-} in normal lattice sites. Protons are displaced off center in H^{2-} centers due to the Jahn-Teller effect. Annealing experiments show that the thermoluminescence peak at around 65 K arises due to the tunneling in the variable distance H^{2-}—F^+ pairs from an excited level at about $E=75$ meV above the ground level of the H^{2-} center. A broad peak centered at about 1.3 μm occurs in the photostimulation spectrum, which corresponds to the optical ionization of the H^{2-} centers.

I. Introduction

Yellow-colored (thermochemically reduced) CaO crystals exhibit bright orange afterglow over a wide temperature range after being excited with light into the F absorption band which peaks at 400 nm [1]. The recombination luminescence of undoped crystals has been related to F centers ionized by light [2]. Relevant hole centers are thus F^+ centers, yet the nature of electron traps related to the two main thermoluminescence glow peaks (below 100 K and above 300 K [3]) has not been cleared unambiguously. Chen and others [3,4] have found arguments stemming from infrared spectra and kinetic measurements for electrons being trapped in the form of the H^{2-} ions substituting oxygen ions in the lattice. That model has been confirmed for traps stable up to the room temperature [5]. The same model has been proposed for shallow traps, which assignment is based on ESR measurements [6]. In the case of MgO, the filled shallow electron traps were identified as H^{2-} ions through low temperature ESR spectra [7], and a different kind of hydrogen trap denoted as $[H_x^-]^0$ was made responsible for the room temperature phosphorescence [8]. Several kinds of hydrogen traps were also found in doped CaO crystals. In highly colored CaO : Mg crystals a hydrogen-related center of intermediate thermal stability giving the 180 K thermoluminescence peak was identified by its ESR spectrum [9]. After X-irradiation of CaO crystals, two paramagnetic impurity-stabilized interstitial hydrogen defects have been found: one near Li^+ [10] and the other near Mg^{2+} [11] ion.

Electron transfer from F centers to electron traps above 60 K proceeds via conduction band upon thermal ionization of the excited states of the F center [2]. At lower temperatures electron tunneling from the excited states of the F and F_A centers to the neighboring F^+ or F_A^+ centers has been found [12–15].

* Eesti Teaduste Akadeemia Keemilise ja Bioloogilise Füüsika Instituut (Institute of Chemical Physics and Biophysics, Estonian Academy of Sciences). 200001 Tallinn, Rävala pst. 10. Estonia.

A clear correlation between ESR and infrared spectra of the shallow hydrogen centers as well as with the low temperature luminescence is still lacking. Below, we shall give new data on paramagnetic and luminescence properties of undoped yellow-colored CaO crystals which show the presence of F^+—H^{2-} pairs at liquid helium temperatures.

Recently a paper of Orera et al. [16] appeared where the ESR spectrum of shallow hydrogen traps in CaO was investigated. The experimental data presented in [16] practically coincide with ours, whereas the interpretation of the nature of the defect is somewhat different (see also [17, 18]).

II. Experimental

Arc fusion-grown CaO crystals of 99.95 per cent purity were obtained from W. and C. Spicer, Ltd. Experimental samples were cleaved from yellow-colored regions which exhibited orange afterglow when exposed to daylight. The concentration of electrons trapped at anion vacancies was about 10^{18} cm^{-3} as estimated from optical absorption spectra, the F band (400 nm) being usually twice as strong as the F^+ band (340 nm). Most ESR measurements were performed on a $6.5\times2.8\times1.5$ mm^3 sample (No. 15) with cleaved (100) surfaces. One sample (No. 16) was prepared for rotating around the ⟨110⟩ axis by grinding the two (110) surfaces in subsequent mixtures of grinding powders and castor oil on a glass plate.

Samples preheated above 420 K and kept in the dark during cooling to liquid helium temperature in the X band cavity, exhibited only a F^+ line at $g=2.0001$ and much weaker signals of manganese impurity over a field interval of 3290 ± 500 Gauss.

Optical excitation of crystals was performed either with a high pressure Hg lamp, the radiation of which was filtered in band-pass glass filters and contained mainly lines at 365, 405 and 436 nm, or with a pulsed nitrogen laser (337.1 nm). In the latter case F centers were excited due to the reabsorption of the fluorescence of F^+ centers.

An Oxford Instruments continuous flow cryostat CF 204 together with the ITC 4 temperature controller were used for spectral measurements. Absorption spectra were measured with a Carl Zeiss (Jena) Specord M 40 spectrophotometer. Luminescence spectra during the annealing experiments were dispersed with a small grating monochromator (3nm·mm^{-1}) driven with a step motor which gave a maximum scanning speed of 30 nm·s^{-1}. Luminescence intensity was measured with a multialkali cathode photomultiplier and stored in the multichannel analyzer NTA 1024 (EMG, Hungary).

The electron paramagnetic spectra and their evolution were measured in the X band H_{102} cavity of the phase-sensitive (100 kHz) ERS 230 spectrometer (Acad. Sci. of GDR). To calibrate the magnetic field, the CaO F^+ center resonance line ($g=2.0001$ [11]) and the readings of the frequency meter were used. Magnetic field scan amplitude (±10 Gs) was calibrated in a separate measurement with ^{53}Cr hyperfine spectrum of Cr^{3+} center in powdered MgO sample supplied by manufacturer. Low temperature measurements were performed in the Oxford Instruments ESR 10 continuous flow cryostat. The objects were sealed in a He atmosphere into a quarts tube of 200 mm length and 4 mm o. d. The cavity had two optical accesses: one from the side orifice which we equipped with a solid organic glass lightpipe, and the other along the quartz tube which contained the crystal and the upper end of which we sealed with a quartz window, attaching it to a plastic fibre bundle. Both accesses might serve either as excitation or registration channels.

Temperature measurement is a special problem in our ESR cryostat, because the thermocouple is in the helium flow surrounding the quartz tube with crystal. We made calibration experiments with the equipment where the crystal specimen was replaced by a 0.25 Watt carbon resistor. Thermocouple readings above 20 K proved to have confidence at ± 1 K level, yet below 20 K the uncertainty was greater. We believe that the spectral measurements with the crystal at minimum temperature (which we refer to as LHeT) were made at 3 K; this temperature, though uncertain was quite reproducible as the measured line intensities show. Less reproducible results were obtained by rotating the crystal. The quartz tube attachment was not centered very well: while rotating, its cold tip made slight side movements which caused unsteadiness of the line intensities resulting from temperature variations.

Annealing experiments were performed using the Oxford Instruments ITC 4 temperature controller. A heating up to the temperature T_k at a rate of 0.2 $K \cdot s^{-1}$ was followed by abrupt cooling, during which the thermoluminescence glow died out in a few seconds, and measurement of the ESR spectrum at LHeT. After that the temperature was set at about $T = 25$ K by regulating the speed of pumping the gaseous helium through the cavity, and the heater power supply was switched on for a new cycle with $T_{k+1} = T_k + 5$ K.

III. Results

A. ESR spectra of CaO irradiated at LHeT

After irradiating a yellow CaO crystal with light into F band at LHeT, a group of ESR lines appeared close to the F^+ line ($g = 2.0001$). These lines had not been described in literature. The intensities and positions of the lines in the spectrum depend on crystal orientation. This is shown in Fig. 1 for the magnetic field rotating in the (010) crystallographic plane. We have interpreted this ESR line pattern as belonging to a $S = 1/2$ defect with the tetragonal symmetry and the hyperfine splitting by a spin $I = 1/2$ nucleus. To do that (see Appendix) we used the theory of first-order forbidden transitions for a system with anisotropic g-factor and hyperfine coupling A [19–21]. The forbidden $\Delta m_I = \pm 1$ lines arise due to the anisotropic dipole-dipole coupling of the nuclear spin and electron spin which, combined with the nuclear Zeeman term $g_n \beta_n H \cdot I$ of the comparable magnitude, give rise to off-diagonal elements between the nuclear spin states. This is the reason why we saw four groups of lines instead of two, which is usual for a $I = 1/2$ system. To fit the experimental data we used the hamiltonian

$$H_0 = \beta H \cdot g \cdot S + S \cdot A \cdot I - g_n \beta_n H \cdot I, \qquad (1)$$

where $g_\parallel = 1.9996 \pm 0.0001$, $g_\perp = 2.0005 \pm 0.0001$, $A_\parallel = 40.3 \pm 1.6$ MHz, $A_\perp = 20.9 \pm 0.8$ MHz, $g_n = 5.6 \pm 0.2$. Second-order contributions from off diagonal S_x, S_y terms were found to be insignificant when compared with the experimental errors. The given value of the nuclear g-factor is very close to that of the proton, and we shall call the lines henceforth «new hydrogen lines».

Rotational diagram around the [110] axis has given a pattern which was in qualitative agreement with the tetragonal symmetry of the center.

The angular dependence of the intensity of some lines is given in Fig. 2. The absolute value for these lines suffered much stronger variations because they were affected by temperature. The line at 3295.7 Gs,

which corresponds to a center preserving its orientation of 90° to the field during the rotation and should therefore have a constant intensity (as an allowed transition) if the temperature did not change, was used to normalize the intensity of other two lines.

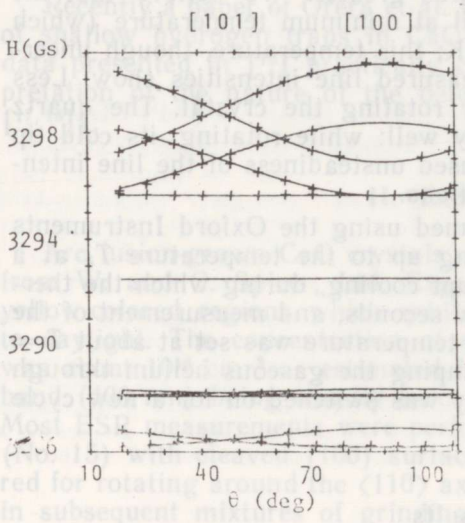

Fig. 1. Angular dependence of the H^{2-} ESR spectrum at LHeT when the magnetic field is rotated in the (010) plane. Central line is the F^+ center resonance. Solid lines represent the calculated positions. $\nu_0 = 9217$ MHz.

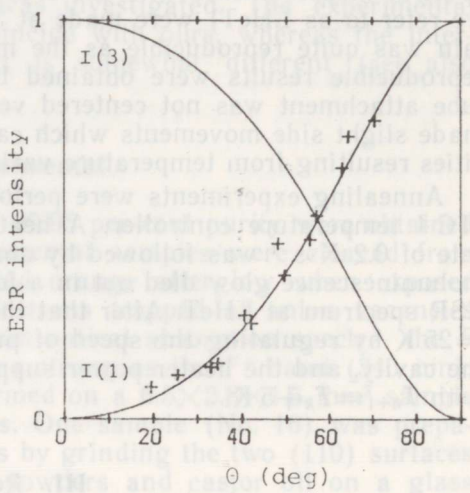

Fig. 2. Angular dependence of the H^{2-} ESR line intensities at LHeT. Crosses are normalized intensities $I(2)$ of the inner pair strong-field components. Solid lines correspond to the formula (A12).

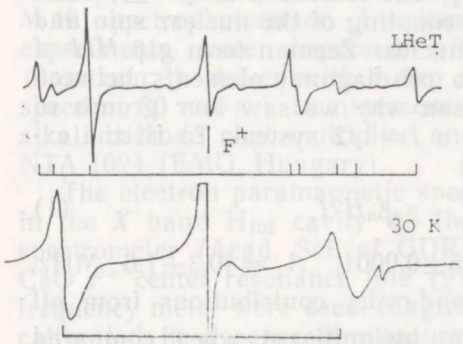

Fig. 3. First derivative ESR spectra of the H^{2-} center (shown by sticks) when the magnetic field is about 19° out of [001] direction in (010) plane. The 30 K spectrum is measured with increased microwave power and spectrometer gain.

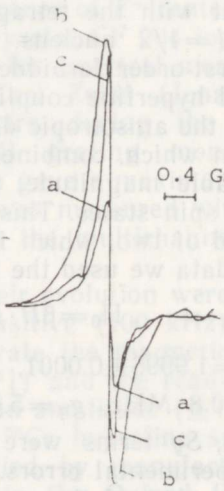

Fig. 4. F^+ resonance line at LHeT: *a* — before irradiation, *b* — after irradiation at around $\lambda = 400$ nm and *c* — being heated subsequently to 100 K.

When the temperature of the crystal was raised, the new hydrogen lines in the ESR spectrum began to shift and amalgamate. At 30 K there remained a simple two-line spectrum of an isotropic center with $g = 2.0002 \pm 0.0001$ and $A = 29 \pm 1$ MHz. The line width which was below 200 mGs (peak to peak) at LHeT grew up to about 600 mGs at 30 K (see Fig. 3). These changes were reversible, and after cooling the crystal to LHeT the picture was restored. Annealing at still higher temperatures (e. g. 3 minutes at 78 K) leads to irreversible loss of the new hydrogen lines. Detailed measurements of the thermal stability of the paramagnetic center will be described in the next section.

The behavior of the F^+ line deserves special attention (Fig. 4). When the crystal was warmed above 420 K and kept in the dark during the cooling, the narrow (peak to peak width 140 mGs) F^+ line was measured at LHeT. After irradiation into the F band, which created new hydrogen lines, the F^+ line grew in its intensity and became wider (180 mGs). After being annealed until new hydrogen lines disappeared, the F^+ line nearly retained its amplitude but its «extra» width disappeared. The greater part of the line narrowing occurred soon when we kept the crystal in the dark at LHeT until the luminescence afterglow has decayed.

Evaluating those results as an expression of $F \leftrightarrow F^+$ conversion, one must bear in mind that, due to large spin-lattice relaxation time, the F^+ line is saturated at LHeT while the new hydrogen lines are not. Therefore, the intensity changes of the lines cannot be taken as proportional to the number of centers — the «wings» are less saturated. A crude estimation based on room temperature intensity of the F^+ line and low temperature intensities of the new hydrogen lines has shown that the number of F^+ centers was by 1—2 orders of magnitude greater than the number of created hydrogen centers.

B. Luminescence of CaO crystals

Our spectral measurements have shown that the emission spectrum of yellow-colored CaO crystals below 100 K consisted of a single band between 420 and 780 nm, with its peak at 610 nm and spectral width of 37 nm at half maximum. The same band was dominant in the fluorescence during excitation with light into the F band as well as in the phosphorescence and the stimulated luminescence after irradiation into F band, independent of whether the stimulation was by heat (the glow peak at 65 K) or by light (e. g. with laser emitting at 830 nm). This spectrum arises when the $^3T_{1u} \rightarrow {}^1A_{1g}$ transition takes place in the F center (see, e. g. [2]), and this also occurs when the electron was taken away by previous illumination and had to recombine with the F^+ center.

The glow curve after irradiating the crystal at LHeT had a peak at 65 K (at heating rate 0.2 $K \cdot s^{-1}$) and an asymmetric shape (see Fig. 5). When the crystal was irradiated at 77 K, then cooled to LHeT and heated (at the same rate), a more symmetric glow peak occurred at 88 K (Fig. 5). To check whether the above behavior could be caused by more than one kind of shallow electron traps, the properties of those traps have been elucidated from a logarithmic plot of the ratio of the luminescence intensity to the remaining light sum [22] (see Fig. 6). For the low temperature peak a straight line approximates the rising part of the glow curve giving an activation energy of $E_1 = 50$ meV and a very small preexponential factor, $p_{01} = 200$ s^{-1}. For the peak at around 88 K we got a little higher energy of $E_2 = 55$ meV and still lower value of $p_{02} = 20$ s^{-1}.

A more detailed fractional thermoluminescence investigation including isothermic ESR line intensity measurements of the number of new hydrogen centers has shown that the light sum decays parallel to the number of the paramagnetic hydrogen centers (Fig. 7), thus demonstrating that these centers are responsible for all the thermoluminescence below 100 K. Every fractional glow curve was also used to determine the E and p_0 values of the traps. The values were somewhat higher than had been obtained from complete thermoluminescence curves, yet the overall characteristics were the same: the activation energy was nearly constant over the whole temperature interval ($E = 75 \pm 5$ meV), and the frequency factor diminished considerably towards higher temperatures (see Fig. 8).

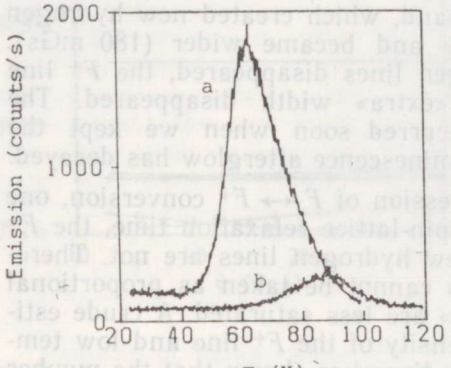

Fig. 5. CaO glow curves after irradiation at LHeT (*a*) and 77 K (*b*).

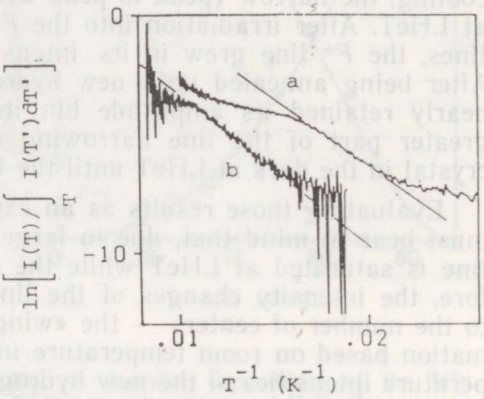

Fig. 6. Logarithmic plot of the glow curves *a* and *b* from Fig. 5. Straight lines represent the first-order kinetics.

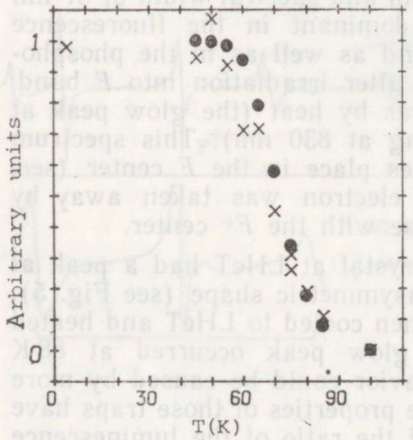

Fig. 7. Sum of the H^{2-} ESR lines peak-to-peak derivative heights measured at LHeT (crosses) and the remaining *F* center luminescence light sum (circles).

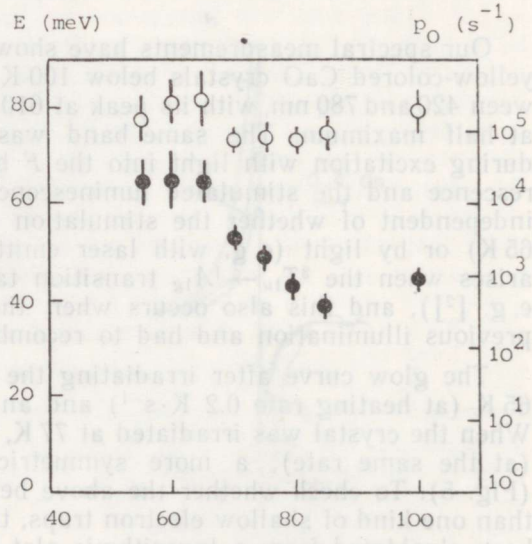

Fig. 8. Activation energy E (opened circles) and pre-exponential factor p_0 (filled circles) obtained from fractional glow curves.

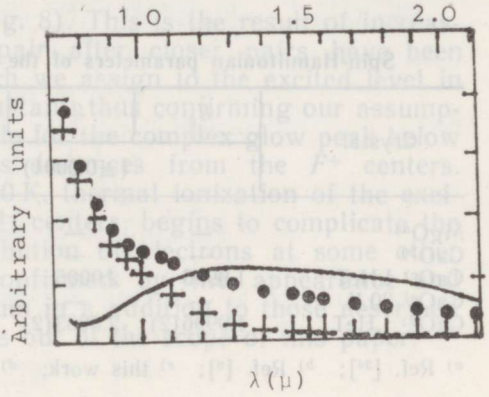

Fig. 9. Stimulation spectra of the F band luminescence in a CaO crystal at LHeT. Dots are for the F-irradiated crystal, crosses after heating to 100 K and solid line represents their difference.

Photostimulated luminescence of CaO crystals, previously irradiated into the F band, revealed a spectral region where the shallow traps have a wide absorption band. This is shown in Fig. 9 where stimulation spectra measured before and after heating the crystal up to 100 K are depicted. The difference spectrum with a maximum at about 1300 nm represents the shallow traps, the absorption band of which overlaps with the long wavelength tail of the spectral band peaking at 520 nm which represents more stable electron traps [5]. Electrons could be transferred between shallow and stable traps by stimulating the crystal with light of suitable wavelength, λ: at $\lambda \geqslant 800$ nm the intensity of new hydrogen lines in the ESR spectrum diminished, while at $\lambda \leqslant 700$ nm the lines grew higher.

IV. Discussion and conclusions

The closest nuclear g factor value to our experimental result $g_n = 5.6 \pm 0.2$ is that of the proton, $g_p = 5.59$. The next 100 per cent abundant $I = 1/2$ nucleus is ^{19}F with $g_n = 5.26$. Hydrogen impurity is expected to be present in hygroscopic calcium oxide crystals due to the thermal decomposition of hydroxil ions during the crystal growth. The similarity between CaO and MgO is another argument supporting the assignment of the trap to the hydrogen impurity, most probably with two additional electrons when filled (paramagnetic). The new feature we found at low temperatures was the low symmetry of the hydrogen center in CaO (see Table 1).

Decomposing the hyperfine interaction into the isotropic (a) and anisotropic (b) components

$$a = 1/2(A_{\parallel} + 2A_{\perp}), \qquad b = 1/3(A_{\parallel} - A_{\perp}), \tag{2}$$

we get $a = 27.4$ MHz and $b = 6.5$ MHz. In the point-dipole approximation the distance between the proton and the unpaired electron spin

$$r = (g\beta g_p \beta_n / bh)^{1/3} \tag{3}$$

becomes $r = 2.3$ Å, which is less than half of the lattice constant in CaO, $r_0 = 4.8$ Å [23].

The isotropic hyperfine interaction of the H^{2-} ion in CaO is about 5 times less than in MgO. Theoretical calculations [7] and the superhyperfine splitting with ^{25}Mg isotope [24] have shown that in MgO the H^{2-} ion substitutes the oxygen in the lattice, the symmetry of the center showing that the proton is situated in the central position. In CaO the proton may have an off-center position shifted along a ⟨100⟩ axis which reduces the spin density on the proton. Reversible changes in the ESR spectrum by rising the temperature are due to motional averaging (jumps between identical positions). The 30 K spectrum (identical to that of Tombrello et al. [6]) is isotropic with measured values of g and A (see Table 1) in agreement with the averaged values $\langle g \rangle = 1/3(g_{\parallel} + 2g_{\perp})$ and $\langle A \rangle = 1/3(A_{\parallel} + 2A_{\perp})$.

Table 1.

Spin-Hamiltonian parameters of the H^{2-} defects in MgO and CaO crystals

Crystal	$g_{\parallel}$	$g_{\perp}$	g	$A_{\parallel}$ (MHz)	$A_{\perp}$ (MHz)	A (MHz)
	($\pm$0.0001)					
MgO[a]	—	—	1.9948	—	—	158$\pm$2
CaO[b]	—	—	2.0002	—	—	28.5
CaO[c] LHeT	1.9996	2.0005	—	40.3$\pm$1.6	20.9$\pm$0.8	—
CaO[c] 30 K	—	—	2.0002	—	—	29$\pm$1
CaO[d] LHeT	1.9996(2)	2.0003(2)		41.2$\pm$0.2	21.4$\pm$0.2	—

[a] Ref. [24]; [b] Ref. [6]; [c] this work; [d] Ref. [16].

In [16] the temperature dependence of the ESR spectrum was analysed using a method based on the stochastic Liouville equation and an activation energy of 7$\pm$2 meV was found for jumps between equivalent orientations (90 degree jumps).

Symmetry argument says that the off-center displacement of the proton is not a static lattice defect. If the origin of tetragonal symmetry were a casual impurity or vacancy (e.g. that of the F^+ center), the motion of the proton could not lead to a isotropic spectrum. We assert that the pseudo-Jahn-Teller effect, including $2s$—$2p$ hybridization in H^{2-} ion, is the cause of lowering the symmetry.

An alternative model, denoted as $[H^-Ca^+]^0$, was proposed in [16], where the trapped electron is located on one of the calcium ions (the nearest neighbor to the H^- ion) and no emphasis was made on static shifts of the ions. However, in a rigid lattice the state of lowest energy should be that of the octahedral symmetry, which contradicts the low temperature experimental finding. A cluster calculation (similar to those made for anion defects in MgO [25, 26]) is underway to find the actual wave function of the trapped electron and the equilibrium positions of the ions.

Now we can discuss the role of the hydrogen traps in $F \leftrightarrow F^+$ photoconversion processes. As is known from earlier work (e.g. [2]), photoexcitation below about 50 K does not lead to ionization of the F center. However, hydrogen traps are effectively filled at the lowest temperatures. Electron tunneling to hydrogen traps from the excited F level should be regarded as the trapping process. This is possible for F centers having in some neighborhood one or more anion vacancies filled with H^- ion. The broadening of the F^+ line in the ESR spectrum after irradiation at LHeT shows that the newly-created F^+ center acquires a disturbing neighbor. If the perturbance is caused by the dipole-dipole interaction between the magnetic moments of the F^+ and H^{2-} electron spins, their average distance could be estimated from 6 to 10 lattice constants. This is less than the average distance between F centers. Therefore we can assume that F^+ and H^{2-} centers form isolated pairs, recombination in which is giving phosphorescence at LHeT. About 1/3 of all created H^{2-} centers disappear during this process. The rest can be abolished either by heating or infrared light. Thermoluminescence follows the first-order kinetics during the rising part of the peak. The small value of the pre-exponential factor says that recombination is not a usual thermally activated process with E as the barrier height and p_0 as the frequency of local vibrations. Thermoluminescence rises as a phonon-assisted tunneling process where E is the distance to an excited (vibrational or rotational) state and p_0 is the tunneling matrix element [27], or a somewhat modified quantity [28]. The value of p_0 is even decreasing in the course

of repeated thermal annealing (see Fig. 8). This is the result of increasing the mean barrier width for the pair after closer pairs have been exhausted. The activation energy which we assign to the excited level in the hydrogen trap remained nearly constant, thus confirming our assumption that the hydrogen traps responsible for the complex glow peak below 100 K differ mainly in having various distances from the F^+ centers. However, if temperature rises above 60 K, thermal ionization of the excited F centers and, possibly, also of H^{2-} centers, begins to complicate the luminescence kinetics, as the redistribution of electrons at some other traps becomes essential. This was confirmed by the appearance and growth of the lines in the ESR spectrum in a addition to those described above. Interpretation of these lines lies out of the scope of this paper.

Acknowledgements

The authors are indebted to E. Lippmaa for supporting the work, to V. Hizhnjakov and O. Sild for discussions and to U. Nagel for assistance in experimental work. We thank V. M. Orera for sending the proof version of the paper [16].

Appendix

In this Appendix we calculate the ESR resonance fields and line intensities for the spin system with anisotropic dipole-dipole coupling of the nuclear spin and electron spin for the case when the nuclear Zeeman term has a comparable magnitude with the hyperfine terms. Our treatment is essentially the same as in the book by Gordy [19], except that we shall account for the anisotropy of the electron g factor (see e.g. [21]).

The spin Hamiltonian which describes interaction between the nuclear spin and the electron spin in the presence of the applied field $\vec{H}$ is

$$\mathcal{H}_0=\beta\vec{H}\cdot\hat{g}\cdot\vec{S}+\vec{S}\cdot\hat{A}\cdot\vec{I}-g_n\beta_n\vec{H}\cdot\vec{I}. \tag{A1}$$

Let the $\hat{g}$ and $\hat{A}$ tensor have an axial symmetry (symmetry axis along [001] crystallographic axis) and the same principal axes, the nuclear g factor g_n be isotropic, and the magnetic field be in (010) plane.

First we diagonalize the electron Zeeman term $\beta\vec{H}\cdot\hat{g}\cdot\vec{S}$ by rotating the electron spin reference frame x_e, y_e, z_e about y axis by an angle ψ [22]

$$\tan\psi=\frac{g_\perp}{g_\parallel}\tan\theta, \tag{A2}$$

where θ is the angle between the magnetic field and the defect symmetry axis. The Hamiltonian in the new electron spin coordinates is

$$\begin{aligned}\mathcal{H}_0=g\beta HS'_z+S'_z\left(I_zA_\parallel\frac{g_\parallel}{g}\cos\theta+I_xA_\perp\frac{g_\perp}{g}\sin\theta\right)+\\+S'_x\left(I_xA_\perp\frac{g_\parallel}{g}\cos\theta-I_zA_\parallel\frac{g_\perp}{g}\sin\theta\right)+A_\perp I_yS'_y-\\-g_n\beta_nH(I_z\cos\theta+I_x\sin\theta),\end{aligned} \tag{A3}$$

where $g^2=(g_\parallel\cos\theta)^2+(g_\perp\sin\theta)^2$.

The terms proportional to S'_x and S'_y give rise to second-order corrections and we neglect them. The rest of the Hamiltonian (A3)

$$\mathcal{H}' = g\beta H S'_z + I_z \left(A_{\parallel} \frac{g_{\parallel}}{g} S'_z - g_n \beta_n H \right) \cos\theta + \\ + I_x \left(A_{\perp} \frac{g_{\perp}}{g} S'_z - g_n \beta_n H \right) \sin\theta \tag{A4}$$

we diagonolize by rotating the nuclear spin reference frame x_n, y_n, z_n about y axis by an angle φ, where

$$\tan\varphi = \frac{A_{\perp} \frac{g_{\perp}}{g} S'_z - g_n \beta_n H}{A_{\parallel} \frac{g_{\parallel}}{g} S'_z - g_n \beta_n H} \tan\theta. \tag{A5}$$

The hamiltonian, diagonal in both electron spin and nuclear spin states, is

$$\mathcal{H} = g\beta H S'_z + \left[\left(A_{\parallel} \frac{g_{\parallel}}{g} S'_z - g_n \beta_n H \right)^2 (\cos\theta)^2 + \right. \\ \left. + \left(A_{\perp} \frac{g_{\perp}}{g} S'_z - g_n \beta_n H \right)^2 (\sin\theta)^2 \right]^{1/2} \cdot I'_z. \tag{A6}$$

Suppose that $I = S = 1/2$. Let

$$A_- = \left[\left(A_{\parallel} \frac{g_{\parallel}}{g} - 2 g_n \beta_n H \right)^2 (\cos\theta)^2 + \left(A_{\perp} \frac{g_{\perp}}{g} - 2 g_n \beta_n H \right)^2 (\sin\theta)^2 \right]^{1/2},$$

$$A_+ = \left[\left(A_{\parallel} \frac{g_{\parallel}}{g} + 2 g_n \beta_n H \right)^2 (\cos\theta)^2 + \left(A_{\perp} \frac{g_{\perp}}{g} + 2 g_n \beta_n H \right)^2 (\sin\theta)^2 \right]^{1/2}. \tag{A7}$$

ESR line positions and intensities for the defect parallel ($\theta = 0°$) and perpendicular is such that

θ	φ_u	φ_l	$H(1)$	$H(2)$
$0°$	$0°$	$0°$	$\frac{1}{g_{\parallel}\beta}(h\nu_0 - h\nu_n)$	$\frac{1}{g_{\parallel}\beta}(h\nu_0 + h\nu_n)$
$90°$	$-90°$	$+90°$	$\frac{1}{g_{\perp}\beta}\left(h\nu_0 - \frac{1}{2}A_{\perp}\right)$	$\frac{1}{g_{\perp}\beta}\left(h\nu_0 + \frac{1}{2}A_{\perp}\right)$

Using this notation we can write four eigenvalues of the Hamiltonian (A6). Two in the upper electron spin state $S'_z = +1/2$ are

$$E_u(+) = \frac{1}{2} g\beta H + \frac{1}{4} A_-,$$
$$E_u(-) = \frac{1}{2} g\beta H - \frac{1}{4} A_-, \tag{A8}$$

and two in the lower electron spin state $S'_z = -1/2$ are

$$E_l(+) = -\frac{1}{2} g\beta H + \frac{1}{4} A_+,$$
$$E_l(-) = -\frac{1}{2} g\beta H - \frac{1}{4} A_+. \tag{A9}$$

Eigenstates of the Hamiltonian (A6) may be expanded in the nuclear spin states $\left|+\frac{1}{2}\right\rangle$ and $\left|-\frac{1}{2}\right\rangle$ (quantization axis parallel to $\vec{H}$) by simple rules (3-dimensional rotation of spin $\frac{1}{2}$ wave functions). Disregarding the part of the wave function which depends only on electron spin coordinates we get

$$|+\rangle_u = \cos\frac{\varphi_u}{2}\left|+\frac{1}{2}\right\rangle + \sin\frac{\varphi_u}{2}\left|-\frac{1}{2}\right\rangle,$$
$$|-\rangle_u = -\sin\frac{\varphi_u}{2}\left|+\frac{1}{2}\right\rangle + \sin\frac{\varphi_u}{2}\left|-\frac{1}{2}\right\rangle,$$
$$|+\rangle_l = -\sin\frac{\varphi_l}{2}\left|+\frac{1}{2}\right\rangle + \cos\frac{\varphi_l}{2}\left|-\frac{1}{2}\right\rangle, \tag{A10}$$
$$|-\rangle_l = \cos\frac{\varphi_l}{2}\left|+\frac{1}{2}\right\rangle + \cos\frac{\varphi_l}{2}\left|-\frac{1}{2}\right\rangle,$$

where the rotation angle φ (A5) is different for the upper and the lower electron spin states (φ_u and φ_l, resp.) due to the difference in the local magnetic fields produced by the electron spin magnetic moment on the nucleus.

Table A1

($\theta = 90°$) to the applied field $\vec{H}$ when the splitting $h\nu_n$ of the nuclear spin levels $\frac{1}{2}A_\perp < h\nu_n < \frac{1}{2}A_\parallel$

$I(1) = I(2)$	$H(3)$	$H(4)$	$I(3) = I(4)$
0	$\frac{1}{g_\parallel \beta}\left(h\nu_0 + \frac{1}{2}A_\parallel\right)$	$\frac{1}{g_\parallel \beta}\left(h\nu_0 - \frac{1}{2}A_\parallel\right)$	1
1	$\frac{1}{g_\perp \beta}(h\nu_0 + h\nu_n)$	$\frac{1}{g_\perp \beta}(h\nu_0 - h\nu_n)$	0

Thus we have four resonance fields corresponding to four possible transitions between the lower and the upper electron spin states

$$
\begin{aligned}
|+\rangle_l \rightarrow |+\rangle_u: \; H(1) &= \frac{1}{g\beta}\left[h\nu_0 - \frac{1}{4}(A_- - A_+) \right], \\
|-\rangle_l \rightarrow |-\rangle_u: \; H(2) &= \frac{1}{g\beta}\left[h\nu_0 + \frac{1}{4}(A_- - A_+) \right], \\
|+\rangle_l \rightarrow |-\rangle_u: \; H(3) &= \frac{1}{g\beta}\left[h\nu_0 + \frac{1}{4}(A_- + A_+) \right], \\
|-\rangle_l \rightarrow |+\rangle_u: \; H(4) &= \frac{1}{g\beta}\left[h\nu_0 - \frac{1}{4}(A_- + A_+) \right],
\end{aligned}
\tag{A11}
$$

where ν_0 is the spectrometer frequency.

If the g factor anisotropy is small, its effect on the line intensities is negligible [22] and we may write the normalized line intensities as

$$
\begin{aligned}
I(1) = I(2) &= \left| \cos\frac{\varphi_l}{2}\sin\frac{\varphi_u}{2} - \cos\frac{\varphi_u}{2}\sin\frac{\varphi_l}{2} \right|^2, \\
I(3) = I(4) &= \left| \cos\frac{\varphi_l}{2}\cos\frac{\varphi_u}{2} + \sin\frac{\varphi_u}{2}\sin\frac{\varphi_l}{2} \right|^2.
\end{aligned}
\tag{A12}
$$

If the crystal is oriented so that the defect symmetry axis is parallel or perpendicular to the applied magnetic field, the spin Hamiltonian parameters may be determined exactly (Table *A1*). The signs of the principal elements $A_\parallel$ and $A_\perp$ of the hyperfine coupling tensor A cannot be specified, but they must be the same (both plus or both minus). Note that for this defect at X band frequencies a special case occurs occasionally: for the defects parallel to the applied magnetic field the local electron field on nucleus $A_\parallel/(2g_n\beta_n)$ is greater than the absolute value of the applied field H and for the defects perpendicular to the applied field the local field is smaller: $A_\perp/(2g_n\beta_n) < H$. This is the reason why there is an orientation angle (either 0° or 90°) for every resonance where the line is forbidden.

REFERENCES

1. *Henderson, B., and Wertz, J. E.* Defects in the Alkaline Earth Oxides. London, Taylor & Francis Ltd., 1977.
2. *Welch, L. S., Hughes, A. E., and Summers G. P.* J. Phys. C: Solid St. Phys., 1980, **13**, 1971.
3. *Summers G. P., Chakrabarti, K., and Chen, Y.* Phys. Rev., 1984, B**29**, 5878.
4. *Gonzalez, R., Summers, G. P., and Chen, Y.* Phys. Rev., 1984, B**30**, 2112.
5. *Orera, V. M. and Chen, Y.* Phys. Rev., 1987, B**36**, 1244.
6. *Tombrello, J., Tohver, H. T., and Chen, Y.* Bull. Amer. Phys. Soc., 1986, **31**, 529.
7. *Tombrello, J., Tohver, H. T., Chen, Y., and Wilson, T. M.* Phys. Rev., 1984, B**30**, 7374.
8. *Orera, V. M. and Chen, Y.* Phys. Rev., 1987, B**36**, 6120.
9. *Boas, J. F. and Pilbrow, J. R.* Phys. Rev., 1985, B**32**, 8258.
10. *Orera, V. M., Alonso, P. J., Sanjuán, M. L., and Alcalá, R.* Phys. Rev., 1989, B**39**, 7982.
11. *Sanjuán, M. L. and Orera, V. M.* J. Chem. Phys., 1986, **85**, 4254.
12. *Ahlers, F. J., Lohse, F., and Spaeth, J. M.* Solid State Commun., 1982, **43**, 321.

13. *Vreeker, R., Kuzakov, S., and Glasbeek, M.* Solid State Commun., 1985, **55**, 1039.
14. *Welch, L. S., and Hughes, A. E.* J. Phys. C: Solid St. Phys., 1980, **13**, 5801.
15. *Henderson, B. and McDonagh, Colette M.* J. Phys. C: Solid St. Phys., 1980, **13**, 5811.
16. *Orera, V. M., Sanjuán, M. L., and Chen, Y.* Phys. Rev., 1990, B**42**, 7604.
17. *Orera, V. M., Sanjuán, M. L., and Chen, Y.* Radiation Effects and Defects in Solids, 1991, **119—121.**
18. *Rõõm, T. and Liidja, G.* Radiation Effects and Defects in Solids. 1991, **119—121**, 855.
19. *Gordy, W.* Theory and Applications of Electron Spin Resonance, Techniques of Chemistry. XV, New York, John Wiley and Sons, 1980, 179—191.
20. *Miyagawa, I. and Gordy, W.* J. Chem. Phys., 1960, **32**, 255.
21. *Abragam, A. and Bleaney, B.* Electron Paramagnetic Resonance of Transition Ions. Oxford, Clarendon Press, 1970. Chap. III.
22. Антонов-Романовский В. В. Изв. АН СССР. Сер. физ., 1946, **10**, 477; V. V. Antonov-Romanovski was the first who proposed the method of determining the parameters p_0 and E of the thermally activated recombination probability $p = p_0 \exp(-E/kT)$ from the $\ln[I(T)/\int_T^\infty I(T')dT']$ vs. T^{-1} plot in the case of first-order kinetics and from the $\ln[I(T)/(\int_T^\infty I(T')dT')^2]$ vs. T^{-1} plot in the case of second-order kinetics.
23. *Hite, H. E. and Kearney, R. J.* J. Appl. Phys., 1967, **38**, 5424.
24. *Orera, V. M. and Chen, Y.* Phys. Rev., 1987, **B36**, 5576.
25. *Pandey, R., and Kunz, A. B.* J. Phys. Chem. Solids, 1990, **51**, 929.
26. *Vail, J. M.* J. Phys. Chem. Solids, 1990, **51**, 589.
27. *Sussmann, J. A.* J. Phys. Chem. Solids, 1967, **28**, 1643.
28. *Вихнин В. С.* Физика тв. тела, 1978, **20**, 1340.

Received
Sept. 8, 1991

Toomas RÕÕM, Georg LIIDJA

VESINIKULE HAARATUD ELEKTRONIDE PARAMAGNETILINE RESONANTS JA TERMOLUMINESTSENTS CaO KRISTALLIDES

Aditiivselt värvitud CaO kristallides tekivad vedela heeliumi temperatuuril F-neeldumisribas kiiritamise järel paramagnetilised tsentrid ($S=1/2$, $I=1/2$), millel on tetragonaalne sümmeetria ja mille tuumne g-faktor ($g_N=5{,}6\pm0{,}2$) vastab prootonile. Need tsentrid tekivad elektroni haaramise tagajärjel hapnikku kristallvõre sõlmes asendavale vesiniku ioonile (H^-), kusjuures prooton nihkub H^{2-}-tsentris võresõlmest Jahni-Telleri efekti tagajärjel kõrvale ⟨100⟩ suunas. Madalal temperatuuril tekib CaO kristallides elektroni tunnelüleminekute tagajärjel varieeruva vahekaugusega F^+—H^{2-}-paaride rekombinatsioonluminestsents. Termoluminestsentsi maksimum 65 K piirkonnas on seotud tunnelüleminekuga ergastatud võnkenivoolt, mis asub ligikaudu 75 meV kõrgemal H^{2-}-tsentri põhinivoost.

Тоомас РЫЫМ, Георг ЛИЙДЬЯ

ПАРАМАГНИТНЫЙ РЕЗОНАНС ЗАХВАЧЕННЫХ НА ВОДОРОДЕ ЭЛЕКТРОНОВ И ТЕРМОЛЮМИНЕСЦЕНЦИЯ В КРИСТАЛЛАХ CaO

В аддитивно окрашенных кристаллах CaO в результате облучения в F-полосе поглощения при температуре жидкого гелия возникают парамагнитные центры ($S=1/2$, $I=1/2$) тетрагональной симметрии, имеющие ядерный g фактор ($g_N=5{,}6\pm0{,}2$), соответствующий протону. Эти центры возникают в результате захвата электрона на ионе водорода H^-, замещающем ион кислорода в узле решетки, причем протон из-за эффекта Яна—Теллера смещается из узла в направлении ⟨100⟩. Низкотемпературная рекомбинационная люминесценция окрашенных кристаллов CaO возникает в результате туннельных переходов электрона в парах F^+—H^{2-}, имеющих переменные расстояния. Пик термостимулированной люминесценции при 65 K связан с туннельными переходами с возбужденного колебательного уровня, расположенного около 75 мэВ выше основного уровня H^{2-}-центра.